Electrochimica Acta 575 (2026) 149505

Contents lists available at ScienceDirect

Electrochimica Acta

journal homepage: www.journals.elsevier.com/electrochimica-acta

Extracting kinetic information on the hydrogen evolution on Pt by combining time-resolved microcalorimetry and finite-element modelling

Marco Schönig [a,b,*], Katherine J. Levey [b], Marc T.M. Koper [b], Rolf Schuster [a]

[a] Karlsruhe Institute of Technology, Institute of Physical Chemistry, Kaiserstraße 12, Karlsruhe, 76131, Germany
[b] Leiden University, Leiden Institute of Chemistry, PO Box 9501, Leiden, RA, 2300, Netherlands

ARTICLE INFO

Keywords:
Electrocatalysis
Reaction kinetics
Hydrogen evolution
Platinum
Electrochemical microcalorimetry
Entropy

ABSTRACT

For fast and reversible electrocatalytic reactions, like the hydrogen evolution on Pt in acidic media and in the presence of molecular H_2, it is very challenging to obtain reliable kinetic information from the charge-potential relationship alone. To overcome this issue, we measure the time-resolved heat flux during hydrogen evolution on polycrystalline Pt as complementary information to chronopotentiometric measurements. The interpretation of the data is based on a comparison with a finite element simulation comprising a microkinetic model coupled to mass transport. Using this approach, we estimate the exchange current density to be around 10 – 15 mA cm^{-2}, for both, the Tafel or the Heyrovský reaction being the rate limiting step. We also find that the coverage of the active hydrogen intermediate is low around the equilibrium potential, even in hydrogen saturated solution.

Introduction

Green hydrogen, i.e., hydrogen produced by electrolysis using renewable energy, is a key technology in the energy transition [1]. At the same time, the hydrogen oxidation is the most researched anode reaction for fuel cell applications [2]. However, despite over a century of research, the exact mechanism of these reactions on polycrystalline Pt, the most active electrode material, is still debated. The main issue is that due to the high catalytic activity of Pt the hydrogen evolution (HER) and hydrogen oxidation reaction (HOR) are very reversible. Therefore, HER and HOR rates cannot be separated at low overpotentials, while at high overpotentials, the current is limited by mass-transport and non-kinetic effects [3].

In general, it is assumed that the reaction proceeds via an electrochemical adsorption/desorption step, called the Volmer "V" step (1), that is followed by either a direct reduction/oxidation (Heyrovský "H") step (2) or recombination Tafel "T" step (3):

$$H^+ + e^- + \square \underset{k_{V,b}}{\overset{k_{V,f}}{\rightleftharpoons}} H_{ad} \quad (1)$$

$$H_{ad} + H^+ + e^- \underset{k_{H,b}}{\overset{k_{H,f}}{\rightleftharpoons}} H_2 + \square \quad (2)$$

$$H_{ad} + H_{ad} \underset{k_{T,b}}{\overset{k_{T,f}}{\longleftrightarrow}} H_2 + 2\square \quad (3)$$

where k_i describe the individual forward or backward rate constants and $\square$ symbolizes an available surface site. We want to emphasize that a polycrystalline electrode consists of a plethora of different surface sites, and a uniform reaction mechanism across all sites is hardly expected. However, for most electrodes, we expect that particularly reactive sites will dominate the overall current response, thus dictating the mechanism we observe in electrochemical measurements. Another possibility discussed in literature is that hydrogen could also absorb in a subsurface layer under specific surface sites and thus alter the reaction environment during the reaction [4].

The most common way to extract reaction rates and the mechanism of an electrochemical reaction is the so-called Tafel plot analysis [5]. The Tafel plot describes the relationship between the decadic logarithm of the current and the overpotential. By using the Butler-Volmer equation and assuming a single rate determining step [6], the slope of the Tafel plot contains information on the reaction mechanism [7] and the intercept corresponds to the exchange current density (j_0), i.e., the intrinsic current density of the reaction at zero overpotential [6]. In the absence of hydrogen and thus negligible HOR, a Tafel slope of 30 mV/decade can be found for the HER on polycrystalline Pt at low overpotentials [8]. This is in good agreement with a microkinetic model

* Corresponding author.
E-mail address: m.schonig@lic.leidenuniv.nl (M. Schönig).

https://doi.org/10.1016/j.electacta.2026.149505
Received 28 April 2026; Received in revised form 2 July 2026; Accepted 9 July 2026
Available online 11 July 2026

of the Volmer-Tafel reaction, where the Tafel reaction is rate-determining (VT_{rds}) and the intermediate coverage is small. However, if hydrogen is present in the solution the back reaction cannot be considered negligible due to insufficient mass transport of produced H_2 away from the electrode surface [9,10]. Thus, no region with a constant Tafel slope of 30 mV/dec can be found close to the equilibrium potential [3]. In consequence, simple Tafel analysis cannot be used to obtain the exchange current density for the HER in acidic solution in presence of H_2 due to the ongoing back reaction [10].

As a consequence, to unequivocally determine the reaction mechanism and exchange current density of the HER on Pt, complementary information is necessary. In this regard, we recently presented an alternative approach to determine the exchange current density of fast electrochemical reactions using electrochemical microcalorimetry (ECM) [11]. Using this methodology, we determined j_0 to be around 10 - 17 mA cm^{-2} instead of 1 mA cm^{-2} as typically extracted from Tafel analysis [12]. With regards to the reaction mechanism, Conway and coworkers proposed a methodology analysing the potential decay during galvanostatic pulses to investigate the intermediate H_{ad} coverage as complementary information [13]. Their experiments indicate that close to the equilibrium, even in a H_2 saturated solution, the coverage is still very small. They found that similar to the HER in absence of hydrogen, the VT_{rds} mechanism was dominant at low overpotentials. They further noted that the reaction could in parallel also proceed via the Volmer--Heyrovský mechanism, where the Heyrovský reaction is rate-determining (VH_{rds}), which would start to dominate at higher η. The observation of a low intermediate coverage around E_0 is further underlined by surface-enhanced spectroscopic investigations conducted by Kunimatsu et al. [14]. They were able to resolve the potential dependence of a spectroscopic signature ascribed to H_{ad}, with a small coverage at low overpotential which quickly increases with increasing overpotential. From the coverage-potential relationship they conclude that the reaction proceeds via a VT_{rds}. Recently, also Gibson et al. analysed the coverage-potential relationship determined by surface-enhanced infrared spectroscopy [15]. Similarly to Kunimatsu et al., they found a low intermediate coverage at low overpotentials but concluded on a VH_{rds} mechanism based on the coverage dependence as function of HER current density. They also show that the adsorption of hydrogen, i.e., the Volmer step, is a fast and reversible process that is not rate determining. The results of both spectroscopic studies align well with results of a microkinetic model by Quaino et al., which combines reactant diffusion, the individual reaction steps and adsorbate interactions to simulate HER current in presence of H_2 using a rotating-disk electrode [16]. Their study indicates a VT_{rds} mechanism with a very small contribution of the Heyrovský reaction and a H_{ad} coverage at the equilibrium potential, θ_0, of around 0.18. In summary the current mechanistic understanding is that the second reaction step, either the Tafel or Heyrovský step, is rate limiting in acidic solution.

In this contribution, we demonstrate that measuring the time-resolved heat flux during chronopotentiometric experiments by ECM can serve as complementary information to the charge-potential relationship, allowing us to extract kinetic parameters for the HER in H_2-saturated sulfuric acid solution (pH ≈ 1). For this purpose, we will compare the experimental overpotential and heat flux transients to results of a finite-element simulation employing a microkinetic model of the HER coupled to mass-transport. We will utilize a wide range of simulation parameters for both the VT_{rds} and VH_{rds} reaction pathways. This allows us to propose reasonable exchange current densities and the equilibrium coverage in case of both mechanisms.

Experimental and simulation details

Solutions and materials

All solutions were prepared from 96% sulfuric acid (Merck, Suprapur) using ultrapure water (Sartorius Arium, 18.2 MΩ·cm). For heat calibration, an equimolar 0.1 M solution was prepared from $K_3[Fe(CN)]_6$ and $K_4[Fe(CN)]_6$ (Merck, 99%) and ultrapure water. To ensure clean conditions, the electrochemical cell and all glassware were submerged in a 3:1 mixture of 96% sulfuric acid (Sigma-Aldrich, EMSURE iso) and 30% hydrogen peroxide (Sigma Aldrich, puriss. p.a.) before each experiment and afterwards boiled and rinsed at least 3 times in ultrapure water.

As working electrode thin platinum foils (50 µm, 99.99% Alfa Aesar Premion) were used, while a 0.5 mm Pt wire (99.99%, Wieland Edelmetalle) was used as counter electrode. All potentials are measured against a palladium-hydride reference electrode [17], prepared from a 0.5 mm palladium wire (99.95%, Advent). Please note that in this manuscript we mainly report overpotentials, as described in more detail in the following section.

Electrochemical microcalorimetry

The microcalorimetric measurements were conducted in a home-built calorimeter described elsewhere [18]. The experimental procedure was previously described in ref [11], but key aspects are summarized as follows:

The microcalorimetric cell was assembled under continuous Ar flow to minimize contamination of the Pt surface. Subsequently, the cleanliness of the experimental setup was assessed by a cyclic voltammogram (CV) and the charge in the hydrogen underpotential deposition was used to determine the electrochemically active surface area (ECSA) [19]. A typical CV is given in the supporting information S1. Afterwards, the 0.1 M H_2SO_4 solution was saturated with hydrogen by fixing the potential at a current of around −1.3 mA for at least 10 min. The measurements were started from open-circuit potential (OCP). Under these conditions, the OCP reflects the equilibrium potential of the relevant redox reaction, i.e. the hydrogen evolution/oxidation reaction [6], which was measured to be around −0.059 V vs the Pd-H reference electrode. Starting from the OCP, current pulses with varying duration and amplitude were applied and the corresponding potential change as well as the temperature change at the surface were monitored. After 1 s the cell was switched back to OCP, and the system was rested for another second. By driving the reaction with current pulses we control the charge, i.e., the amount of produced H_2, to stay close to equilibrium conditions. The overpotentials reported in this manuscript are obtained by subtracting the measured potential before the pulse from the overall potential transient. Additionally, the IR-drop was manually subtracted from the data, using the linear relationship between the applied current pulse and the resulting potential jump, by subtracting the sharp potential drop after switching of the current flow [20]. For each experimental setup the thermal response of the setup was calibrated using 2 ms laser pulses. The overall exchanged heat was calibrated using a 0.1 M $K_3[Fe(CN)_6]/K_4[Fe(CN)_6]$ solution, as described in ref [18].

Please note that due to a small offset of around 5 µA in the potentiostat, the applied positive and negative currents are slightly asymmetric. E.g., +155 and −145 µA were applied in the case of a chosen current of 150 µA.

Model and theory

The heat flux $\Phi(t)$ generated during an electrochemical reaction measured with ECM consist of three main contributions: (1) the heat caused by the entropy change of the individual reactions $\Delta_R S_i(t)$, (2) the heat generated by ion transport $\Delta_T S$, and (3) heat generated by the overpotential $\eta(t)$ necessary to drive the reaction:

$$\Phi(t) = \sum_i T r_i(t) \Delta_R S_i(t) + T I_{ext}(t) \Delta_T S + I_{ext}(t)\ \eta(t) \quad (4)$$

where $r_i(t)$is the rate of reaction *i*, *T* the temperature and $I_{ext}(t)$ is the applied current. Both the reaction entropy as well as the overpotential can change with the reaction progress, as they are dependent on the

surface concentration of each species. It can be shown that in the presence of supporting electrolyte $T\Delta_R S_i(t)$ and $\eta(t)$ can be substituted by the Peltier heat and η at the beginning of the pulse, respectively [21]. Furthermore, in the presented experiments concentration changes are small (typically far below 1%, cf. Fig. 3b). Thus, $\Delta_R S_i(t)$ and $\eta(t)$ will not show pronounced variations during the pulse.

It is apparent from eq. (4) that by using a microkinetic model to calculate $r_i(t)$ in principle the individual heat contributions of the different reaction steps could be disentangled. The reaction entropy of the individual reactions and transport entropy can be calculated following the procedures outlined in ref [22] and [23]. The values are summarized in Table S1 of the supporting information.

A one-dimensional finite element model was designed to simulate the time-dependent concentration distributions by solving Fick's second law, as well as the heat flux according to eq. (4), resulting from short current pulses. The microkinetic model is adapted from ref [24].

The transport of ions in the solution was simulated using an ideal solution approximation, with the starting conditions matching the experimental conditions, i. e., 0.1 M sulfuric acid solution. All parameters used in the simulation and a more detailed description of the implementation of the finite-element model are summarized in part S2 of the supporting information. Due to the very small and short current amplitudes that we are using, the concentration changes of H^+ at the surface and the overpotential changes are very small, as will be discussed later. Thus, in this case the effect of mass-transport is quite small, allowing us to neglect migration and convection in the simulation. However, for the investigation of higher current densities, the effects of migration would need to be considered if no supporting electrolyte is used.

The microkinetic model was incorporated using the individual reaction rates r_i resulting from the three elementary reactions 1–3, following the microkinetic model introduced by Lasia in ref [24]. In this model it is assumed that the Butler-Volmer formalism describes the potential dependence of the rate constant and that the adsorption of hydrogen follows a simple Langmuir isotherm. The model further utilizes the condition that the rates of all reactions are zero at the equilibrium potential of the HER E_{eq},

$$r_V = r_H = r_T = 0 \tag{5}$$

which allows us to refer all potentials to E_{eq} and to introduce the overpotential $\eta = E - E_{eq}$.

Following this procedure, the reaction rates of the individual reactions are given by:

$$r_V = k_{V,f}\,(1-\theta)\,\frac{c_H}{c_H^0}e^{-\alpha f\eta} - k_{V,b}\theta e^{(1-\alpha)f\eta} \tag{6}$$

$$r_H = k_{H,f}\,\theta\,\frac{c_H}{c_H^0}e^{-\alpha f\eta} - k_{H,b}(1-\theta)\,\frac{c_{H_2}}{c_{H_2}^0}e^{(1-\alpha)f\eta} \tag{7}$$

$$r_T = k_{T,f}\,\theta^2 - k_{T,b}(1-\theta)^2\frac{c_{H_2}}{c_{H_2}^0} \tag{8}$$

where θ is the surface coverage with H_{ad}, c_i is the concentration of species i near the surface, c_i^0 is the bulk concentration of species i and α is the charge transfer coefficient, which for simplicity is assumed to be 0.5 [25]. Please note that θ in this case refers to the coverage of the reactive hydrogen intermediate, which is generally called overpotential-deposited hydrogen H_{opd}, as opposed to the hydrogen deposited substantially above the standard equilibrium potential of the HER/HOR, i.e., the underpotential-deposited hydrogen H_{upd} [13]. H_{opd} is assumed to be the species detected by IR-spectroscopy [14,15].

The rate constants $k_{V,f}$, $k_{V,b}, k_{H,f}, k_{H,b}$, $k_{T,f}$, $k_{T,b}$ in eq. (6) - 8 resulting from this model are in units of flux, mol m^{-2} s^{-1} and can be used directly in finite-element simulations. For detailed discussion of the model, we refer to the paper by Lasia [24].

From eq. 5 further follows that only 4 of the 6 rate constants or 3 of the rate constants and the equilibrium coverage θ_0 are independent parameters [24]. We chose to define the forward rate constants and θ_0, such that the corresponding backward rate constants can be calculated as follows:

$$k_{V,b} = k_{V,f}\frac{(1-\theta_0)}{\theta_0} \tag{9}$$

$$k_{H,b} = k_{H,f}\frac{\theta_0}{(1-\theta_0)} \tag{10}$$

$$k_{T,b} = k_{T,f}\left(\frac{\theta_0}{(1-\theta_0)}\right)^2 \tag{11}$$

To reduce the parameter space, we considered only cases, where the reaction proceeds either via the Volmer-Tafel or Volmer-Heyrovský pathway and the second reaction step is rate-determining. The Volmer reaction is assumed to be 100 times faster [16] and the rate constant for the other reaction pathway is set to 0 mol m^{-2} s^{-1}. In this case the rate constant of the rate-determining step can be linked directly to the exchange current density, allowing us to define the rate constant using an experimentally accessible quantity.

We calculated the rate constants for the individual reactions from the exchange current density using:

$$k_{H,f} = \frac{j_0}{2F\,\theta_0} \tag{12}$$

$$k_{T,f} = \frac{j_0}{2\,F\,{\theta_0}^2} \tag{13}$$

COMSOL Multiphysics (Version 6.2) was used to solve equations 4 - 13. A detailed description of the model including the mesh, boundary conditions as well as a discussion of the parameter choices are included in part S2 of the supporting information. The COMSOL generated model report is also provided as a separate file to aid those wishing to adapt the model.

Results and discussion

Experimental measurements

Fig. 1 shows typical experimental results of ECM measurements of the HER/HOR driven by

± 150 μA current pulses (corresponding to 1 mA cm^{-2}) of 20 ms duration; The upper curves in Fig. 1a and 1b shows the respective current pulses. The curves in the row below show the measured overpotential as a function of time; the third row of curves shows the measured heat flux, Φ, resulting from the applied current pulse; finally, the lowest row of curves shows the exchanged heat q, i.e., the integral of the heat flux.

It is readily visible from Fig. 1 that only a small overpotential of around 2.5 – 3 mV is necessary to drive the reaction at ±150 μA for 20 ms. After switching off the current flow at 30 ms, the overpotential quickly relaxes to its initial value signalling that the equilibrium was not measurably perturbed.

Directly upon driving the HER at 10 ms, the heat flux promptly decreases to around −13 μW during the current flow (Fig. 1a). This is also visible as a linear increase of q. After the pulse the heat flux gradually decays to zero in <10 ms. Following this short decay, the overall exchanged heat stays constant at a value of $q_{total} = -275$ nJ. The quick ceding of the heat flux shows that no significantly delayed reaction steps are taking place as no further heat is produced. The same observation can be made for the HOR in Fig. 1b The exchanged heat is slightly larger in the case of the HOR due to the irreversible contribution of the overpotential heat. The overpotential heat always contributes positively to the exchanged heat, leading to less cooling in the case of the HER and

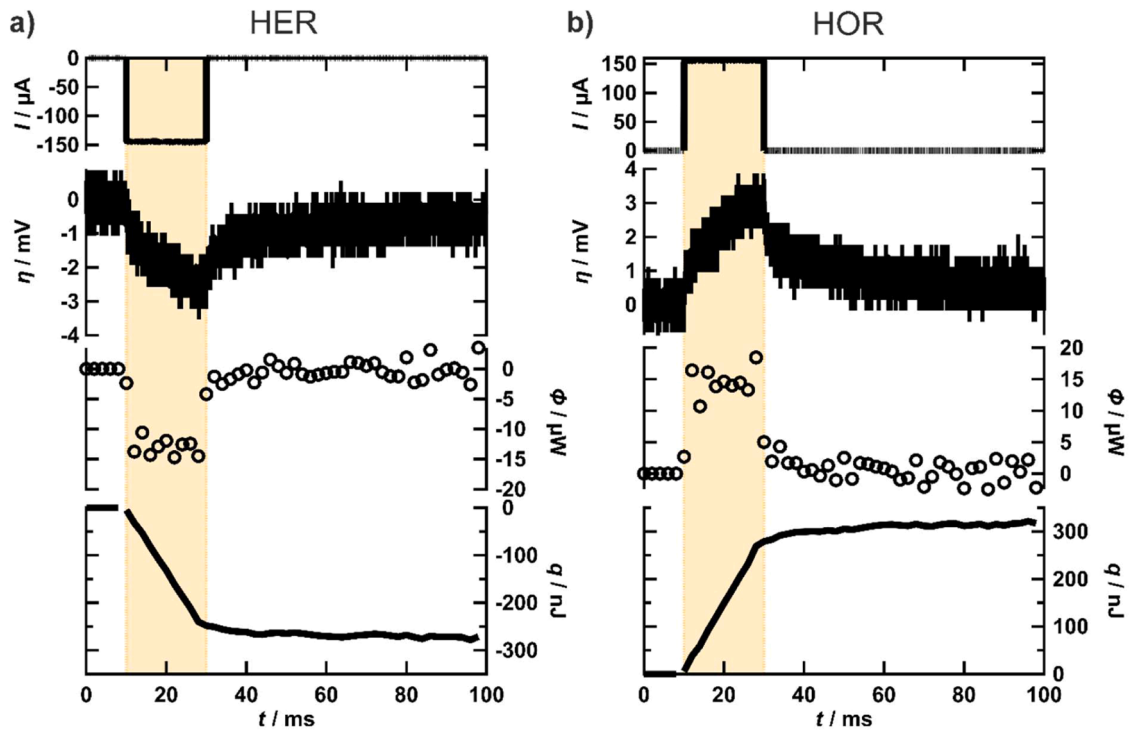

Fig. 1. Experimental data resulting from a 20 ms current pulse of a) −150 µA and b) + 150 µA . The 2nd row shows the overpotential after IR correction, the 3rd row shows the heat flux, and the 4th row shows the exchanged heat, i.e., the integrated heat flux. The shaded yellow area indicates the duration of the current pulse. Before and after the pulse the cell was at OCP.

stronger heating in the case of the HOR [21]. With the theoretical reaction entropy of 67.7 J mol^{-1} K^{-1} and transport entropy of 35.8 J mol^{-1} K^{-1} [23], a value of $q_{theo} = 304$ nJ would be expected for HER. This is in reasonable agreement considering the systematic error of the heat measurement of 2 kJ mol^{-1} [26], which corresponds to 60 nJ, considering the conversion in the experiments in Fig. 1.

Fig. 1 clearly shows that we can measure the heat flux during an electrochemical reaction with µW resolution in 2 ms time intervals. This provides us with two evaluable variables to compare to the microkinetic model, in order to disentangle the contributions of the different reaction steps.

Finite element modelling

As parameters for the microkinetic model, we chose four possible j_0 values between the typically reported value of 1 mA cm^{-2} [12] and the highest observed j_0 in our previous contribution of around 15 mA cm^{-2} [11]. For the equilibrium coverage θ_0 we chose values between 0.01, representative of the low coverage situation observed for the HER in absence of H_2 [7], and 0.7, representative of a highly covered surface. All parameters used in the simulations are summarized in Table 1.

The results of all simulations of the HER and HOR for all 16 parameter combinations for both investigated reaction mechanisms are shown in part S3 of the supporting information (Fig.S3 - S6). To narrow down a reasonable parameter set, we first compare the simulated overpotential with the experimental overpotential (Fig. 2). In the following section, we then analyse the simulated heat flux and compare it to the experimental heat flux and the overall exchanged heat (Fig. 4).

Table 1
Summary of kinetic parameters used in the finite-element modelling.

	j_0 / mA cm^{-2}	θ_0
Parameters used in Simulation	1, 5, 10, 15	0.01, 0.1, 0.3, 0.7

Overpotential

From the simulation we found that the equilibrium H_{ad} coverage has only a minor influence on the overpotential for a given j_0 value and thus we only analyse representative results for $\theta_0 = 0.1$ in Fig. 2.

Fig. 2a shows the simulation results for the Volmer-Tafel mechanism, with the Tafel reaction being the rate determining step (VT_{rds}). It is readily visible that for this mechanism only high enough values of $j_0 = 10$ mA cm^{-2} (red) or $j_0 = 15$ (blue) mA cm^{-2} can explain the very small overpotential observed experimentally. A similar trend can be observed in Fig. 2b for the VH_{rds} mechanism. The analogous plots to Fig. 2 for the HOR are shown in Fig. S7 of the supporting information and yield the same conclusions.

The results presented in Fig. 2 show clearly that by comparing only the experimental charge-potential relationship to the results of the finite-element simulations, no final decision between VT_{rds} and VH_{rds} can be drawn and we cannot conclude on θ_0.

Heat flux and total heat

As additional information to the overpotential, we can obtain the individual contributions to the overall heat flux from our microkinetic model following eq. 4. In Fig. 3a we show the individual heat flux contributions (solid lines) together with the resulting overall heat flux (open circles) from our simulations for the exemplary case of the HER following a VT_{rds} mechanism with $j_0 = 10$ mA cm^{-2} and $\theta_0 = 0.1$. In Fig. 3b we show the concentration change of protons at the surface (left axis) and the coverage change of H_{ad} on the surface (right axis) during the pulse.

Fig. 3a reveals that the irreversible contribution of the overpotential heat (black) to the overall heat flux is very small. For the exemplary chosen VT_{rds} mechanism it is evident that the very fast Volmer step (pink), leads to an immediate cooling of the electrode. As the starting H_{ad} coverage is quite small, the rate of the Tafel reaction is low. The continuous build-up of the reaction intermediate, which can be observed

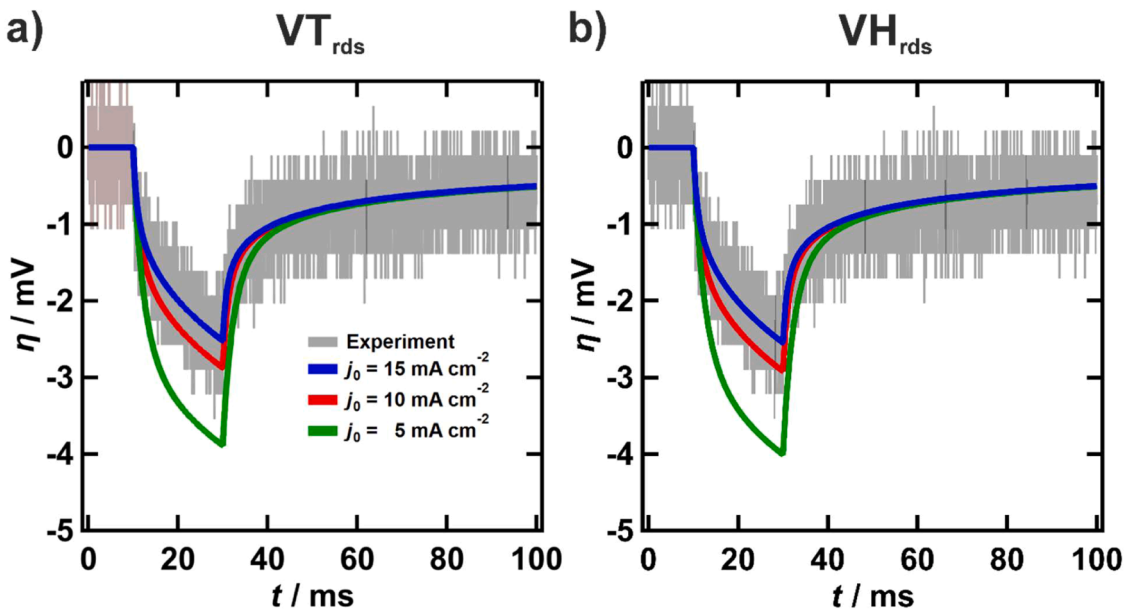

Fig. 2. Experimental overpotential (grey) and simulation results using $j_0 = 5$ mA cm^{-2} (green), 10 mA cm^{-2} (red) and 15 mA cm^{-2} (blue) and $\theta_0 = 0.1$ for a) the VT_{rds} and b) the VH_{rds} mechanism for the HER driven by a 20 ms, −150 µA current pulse.

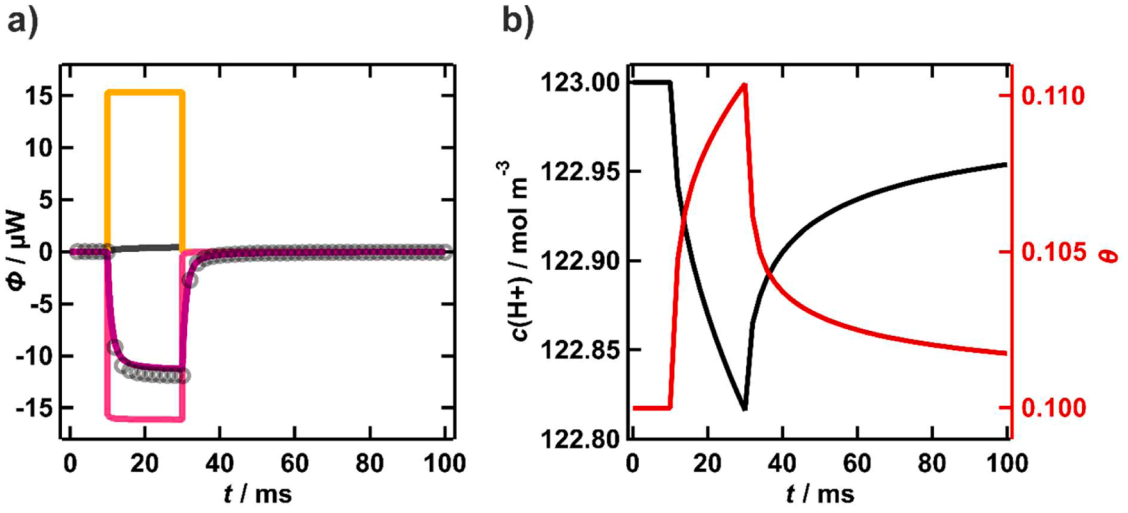

Fig. 3. a) Individual contributions to the heat flux according to eq. 4.: Overpotential heat flux (black), Transport heat flux (orange), heat flux of Volmer reaction (pink) and heat flux of Tafel reaction (purple). The resulting overall heat flux is depicted by grey open circles; b) concentration change of protons at the surface (left axis) and coverage change of H_{ad} on the surface (right axis). The simulation parameters for both figures were $j_0 = 10$ mA cm^{-2} and $\theta_0 = 0.1$.

in Fig. 3b, leads to an increasing heat flux of the Tafel reaction (purple). After the external current flow is switched off, the Volmer reaction instantly cedes, while the built-up H_{ad} coverage is consumed by the Tafel reaction, which keeps producing hydrogen and thereby cooling the electrode even after the end of the current flow. This fits well with the experimentally observed small, delayed heat evolution in Fig. 1. Fig. 3a further shows that in the present case the transport entropy (orange) leads to positive heat flux, which is opposite to that of both elementary reactions. By coincidence, the heat due to transport and due to the Volmer reaction cancel each other almost perfectly. Thus, in cases when neither reaction is fast enough to contribute a significant cooling at the start of the pulse, an initial heating might be observable. The results presented in Fig. 3 show that by using finite-element simulation we are able to disentangle the heat flux into its individual components.

Applying the outlined procedure, we can reconstruct the heat flux from the simulation of the different reaction mechanisms. Fig. 4 shows the heat flux Φ (Fig. 4a and b) as well as the overall heat, i.e., the heat flux integrated over time, q (Fig. 4c and d), resulting from our simulations. In grey we also show the experimental data from Fig. 1a.

Similar to Fig. 2, for clarity reasons we include only selected simulation results in Fig. 4. Here we chose to present only the data resulting from simulations of $j_0 = 10$ mA cm^{-2}. The simulations using $j_0 = 15$ mA cm^{-2} yield very similar Φ and $q(t)$ transients and lower values (1 and 5 mA cm^{-2}) do not fit the experimentally observed overpotentials well. As discussed above the overall exchanged heat in our experiments is slightly smaller than the expected value. To facilitate the comparison between experiment and simulation, we normalized Φ and q in Fig. 4 to the experimental overall exchanged heat q_{total}. The results of all simulations, also for the HOR, in part S3 of the supporting information, are shown without this normalization.

Fig. 4 demonstrates that θ_0 has a considerable influence on the heat flux even for the same j_0, which is in contrast to the behaviour of the simulated overpotential. In case of VT_{rds} (Fig. 4a) and VH_{rds} (Fig. 4b) a lower θ_0 leads to a faster cooling at the beginning of the pulse ($t = 10$ ms)

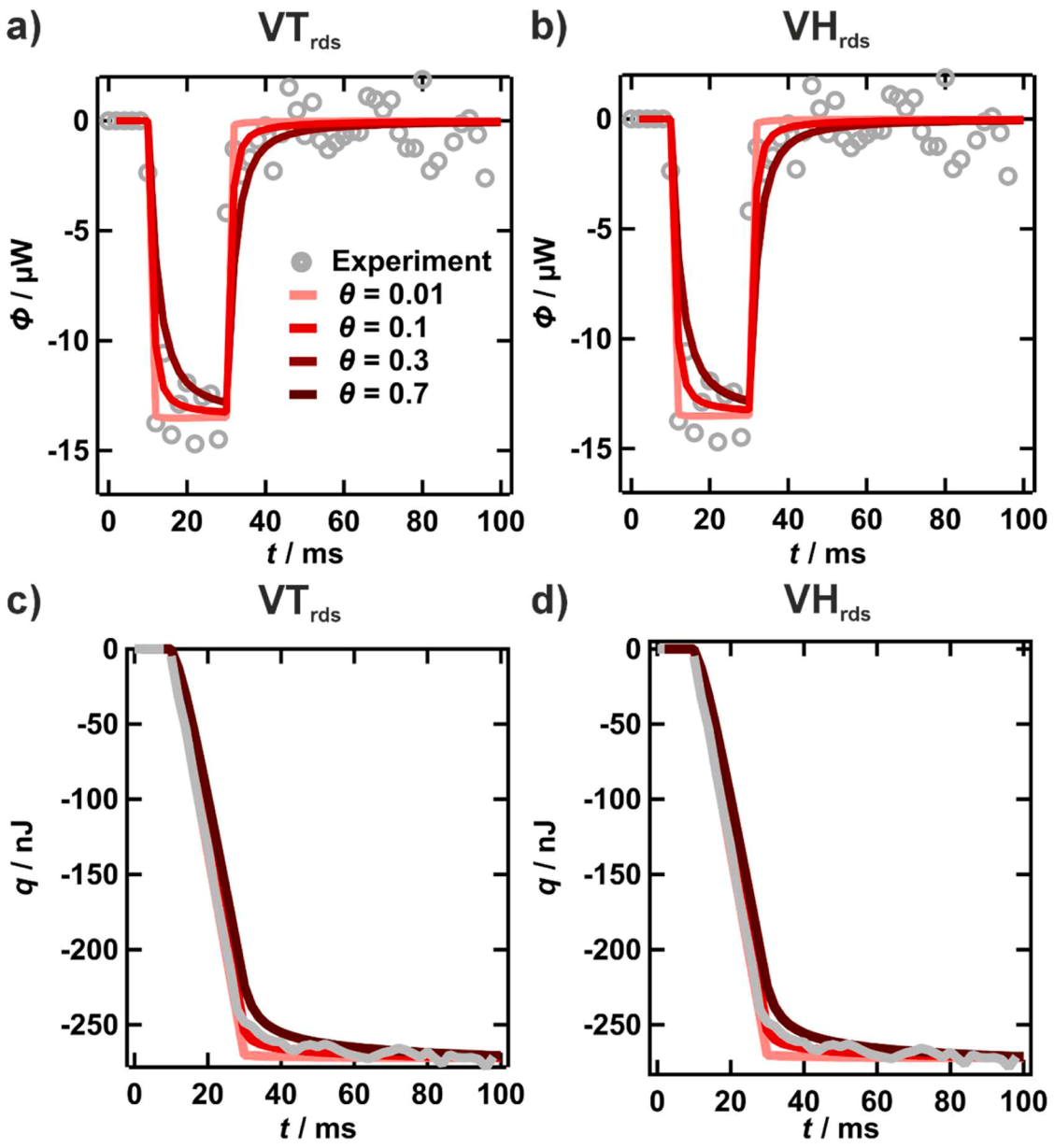

Fig. 4. Experimental heat flux (grey circles) and exchanged heat (grey line) and simulation results for 10 mA cm^{-2}, with different θ_0 values (light red = 0.01, medium red = 0.1, dark red = 0.3, dark brown = 0.7) for both the VT_{rds} (a and c), as well as the VH_{rds} mechanism (b and d).

and no significant heat flux after the end of the pulse ($t = 30$ ms). On the other hand, a higher θ_0 leads to considerable trailing heat flux at the start and after the end of the pulse. It is evident that for both mechanisms VT_{rds} and VH_{rds}, where a nearly identical overpotential response was observed in Fig. 2a and Fig. 2b, also the curves for Φ and q are remarkably similar. The reason for this is that according to eq. 4 the faster reaction, in this case the Volmer reaction, dominates the heat flux. This effect is directly observable for the VT_{rds} mechanism in Fig. 3a.

For both cases, VT_{rds} and VH_{rds}, Fig. 4 reveals that $\theta_0 = 0.01$ would lead to a faster heat exchange than observed in experiment, with basically no delayed heat evolution. In contrast, the simulations with a higher equilibrium coverage show a slower cooling than observed in the experiment. Thus, for the VT_{rds} and VH_{rds} mechanism only the case of $\theta_0 = 0.1$ shows a similar behaviour to the experiment. The same conclusions can be drawn from Fig. S7 of the Supporting Information from the simulation results for the HOR.

From the comparison of experimental overpotential and heat flux, with the results of our finite-element simulation we find that the experimental data can only be explained by a distinct subset of tested kinetic parameters. We find that regardless of the mechanism, the reaction must proceed significantly faster than generally assumed, with j_0 exceeding 10 mA cm^{-2} in line with RDE measurements analysed using the reversible Koutecký-Levich equation, and previous ECM measurements [11]. An overview of j_0 values obtained for the HER on polycrystalline Pt and Pt particles using different techniques was recently given by Tetteh et al., where all values far exceed 1 mA cm^{-2} [27]. We further infer that the HER in 0.1 M H_2SO_4 proceeds either via a VT_{rds} or VH_{rds} mechanism with θ_0 of around 0.1 in agreement with the spectroscopic data by Kunimatsu et al. [14] and Gibson et al. [15], showing that θ_0 is low close to 0 V. The θ_0 value of 0.1 is also very close to results by Quaino et al. [16] who found a dominant VT_{rds} mechanism with $\theta_0 = 0.18$ from their simulations of the current response during an rotating disk experiment from 0.4 V to −0.2 V. However, we are not able to decide whether the VT_{rds} or the VH_{rds} mechanism is dominant, as they both yield a nearly identical ECM response for our measurement conditions.

To further validate our findings, we conducted additional experiments using 10 ms and 30 ms long pulses. In these experiments we kept the overall conversion constant by adjusting the pulse current accordingly. The experimental results together with the corresponding finite element simulations for the most plausible kinetic parameters are shown in Fig. S8 and S9 of the supporting information. For the same conversion we find that q_{total} is very similar, underlining, in accordance with Fig. 3, that the contribution of the overpotential heat to the overall exchanged heat is very small for the investigated current amplitudes. We find that also for the different pulse conditions, only simulations using j_0 exceeding 10 mA cm^{-2} and $\theta_0 = 0.1$ fit well with the experimental data. The comparison for the short 10 ms pulses, suggests that a slightly better agreement could be found by using $j_0 = 15$ mA cm^{-2}.

Conclusion

In this contribution, we demonstrated that the overpotential and heat flux transients from electrochemical microcalorimetry experiments can be accurately modelled using the presented microkinetic model coupled to mass-transport. From this combination, we could significantly narrow down the possible kinetic parameters for the HER at Pt in H_2-saturated sulfuric acid solution (pH ≈ 1). In general, we found the overpotential transients to be more sensitive to j_0 and the heat flux transient to be more sensitive to θ_0. However, with our current approach we were not able to conclude on the dominant reaction pathway, as both the VT_{rds} and VH_{rds} mechanism yield a similar ECM response.

From the analysis of the overpotential transient we find the exchange current density j_0 to be around 10–15 mA cm^{-2} for both the VT_{rds} and VH_{rds} mechanism. This result is consistent with reports that claim that the real exchange current density for the HER on Pt is higher than the typically reported value of 1 mA cm^{-2}. However, we emphasize that the exact exchange current density will always vary depending on active surface sites and electrode composition.

From the heat flux transients, we could infer a θ_0 value of around 0.1 for both mechanisms. This finding agrees well with observations for the HER in absence of Hydrogen, where a VT_{rds} mechanism with low θ_0 is generally accepted. Thus, our findings show that adding hydrogen to the solution does not significantly affect θ_0.

The present study demonstrates the possibilities arising from measuring the heat flux as complementary variable to the charge-potential relationship. We expect that this methodology will be more insightful for slower multi-step reactions, in which the heat fluxes of individual steps are clearly separated, or for reactions whose steps have heat fluxes of opposite sign.

CRediT authorship contribution statement

Marco Schönig: Conceptualization, Data curation, Formal analysis, Funding acquisition, Methodology, Visualization, Writing – original draft. **Katherine J. Levey:** Methodology, Visualization, Writing – original draft. **Marc T.M. Koper:** Resources, Supervision, Validation, Writing – original draft. **Rolf Schuster:** Methodology, Resources, Supervision, Validation, Writing – original draft.

Declaration of competing interest

The authors declare that they have no known competing financial interests or personal relationships that could have appeared to influence the work reported in this paper.

Acknowledgements

M.S. acknowledges funding from 2023 HORIZON-MSCA-PF program under grant agreement No 101147027 and M.T.M.K. acknowledges the award of a Spinoza Grant by the Dutch Research Council (NWO).

Supplementary materials

Supplementary material associated with this article can be found, in the online version, at doi:10.1016/j.electacta.2026.149505.

Procedure to determine the electrochemically active surface area, details of finite element simulation including table of used parameters, simulation results for all parameters, experimental results and simulation results for HOR, experimental and simulation results for different pulse lengths and amplitudes. An exemplary COMSOL model report for the VT_{rds} mechanism is also given as separate file.

Data availability

All data underlying this publication will be made available via data.4tu.nl at https://doi.org/10.4121/c5569c2d-509f-41be-886e-7dc28e495ca8

References

[1] J.A. Turner, Sustainable hydrogen production, Science (1979) 305 (2004) 972–974, https://doi.org/10.1126/science.1103197.
[2] H.-J. Neef, International overview of hydrogen and fuel cell research, Energy 34 (2009) 327–333, https://doi.org/10.1016/j.energy.2008.08.014.
[3] O. van der Heijden, S. Park, R.E. Vos, J.J.J. Eggebeen, M.T.M. Koper, Tafel slope plot as a tool to analyze electrocatalytic reactions, ACS. Energy Lett. 9 (2024) 1871–1879, https://doi.org/10.1021/acsenergylett.4c00266.
[4] J. Wei, Z. He, W. Chen, Y.-X. Chen, E. Santos, W. Schmickler, Catalysis of hydrogen evolution on Pt(111) by absorbed hydrogen, J. Chem. Phys. 155 (2021) 181101, https://doi.org/10.1063/5.0072069.
[5] S. Anantharaj, S. Noda, How properly are we interpreting the Tafel lines in energy conversion electrocatalysis? Mater. Today Energy 29 (2022) 101123 https://doi.org/10.1016/j.mtener.2022.101123.
[6] A.J. Bard, L.R. Faulkner, H.S. White, Electrochemical methods: Fundamentals and Applications, 3rd edition, Wiley, Hoboken, NJ, USA Chichester, West Sussex, UK, 2022.
[7] T. Shinagawa, A.T. Garcia-Esparza, K. Takanabe, Insight on Tafel slopes from a microkinetic analysis of aqueous electrocatalysis for energy conversion, Sci. Rep. 5 (2015) 13801, https://doi.org/10.1038/srep13801.
[8] J.O. Bockris, E.C. Potter, The mechanism of the cathodic hydrogen evolution reaction, J. Electrochem. Soc. 99 (1952) 169, https://doi.org/10.1149/1.2779692.
[9] M. Breiter, H. Kammermaier, C.A. Knorr, Untersuchung der Phasengrenzimpedanz an Edelmetallelektroden im Gebiet der Wasserstoffadsorption I. Aktivierte Platinelektroden, Z. Elektrochem. 60 (1956) 37–47, https://doi.org/10.1002/bbpc.19560600111.
[10] J. Zheng, Y. Yan, B. Xu, Correcting the hydrogen diffusion limitation in rotating disk electrode measurements of hydrogen evolution reaction kinetics, J. Electrochem. Soc. 162 (2015) F1470–F1481, https://doi.org/10.1149/2.0501514jes.
[11] M. Schönig, R. Schuster, Microcalorimetric determination of the exchange current density and the reaction entropy of fast electrochemical processes: hydrogen evolution on Pt, J. Phys. Chem. C 128 (2024) 14649–14653, https://doi.org/10.1021/acs.jpcc.4c03723.
[12] S. Trasatti, Work function, electronegativity, and electrochemical behaviour of metals, J. Electroanal. Chem. 39 (1972) 163–184, https://doi.org/10.1016/S0022-0728(72)80485-6.
[13] B.E. Conway, L. Bai, Determination of adsorption of OPD H species in the cathodic hydrogen evolution reaction at Pt in relation to electrocatalysis, J. Electroanal. Chem. 198 (1986) 149–175, https://doi.org/10.1016/0022-0728(86)90033-1.
[14] K. Kunimatsu, T. Senzaki, G. Samjeské, M. Tsushima, M. Osawa, Hydrogen adsorption and hydrogen evolution reaction on a polycrystalline Pt electrode studied by surface-enhanced infrared absorption spectroscopy, Electrochim. Acta 52 (2007) 5715–5724, https://doi.org/10.1016/j.electacta.2006.12.007.
[15] A.J. Gibson, J.J.T. Shibuya, A. Cuesta, The HER on Pt: revisiting tafel slope analyses when deducing reaction mechanisms, J. Solid. State Electrochem. (2026), https://doi.org/10.1007/s10008-026-06564-6.
[16] P.M. Quaino, M.R. Gennero de Chialvo, A.C. Chialvo, Hydrogen electrode reaction: a complete kinetic description, Electrochim. Acta 52 (2007) 7396–7403, https://doi.org/10.1016/j.electacta.2007.06.030.
[17] M.J. Vasile, C.G. Enke, The preparation and thermodynamic properties of a palladium-hydrogen electrode, J. Electrochem. Soc. 112 (1965) 865, https://doi.org/10.1149/1.2423713.
[18] S. Frittmann, V. Halka, C. Jaramillo, R. Schuster, An improved sensor for electrochemical microcalorimetry, based on lithiumtantalate, Rev. Sci. Instr. 86 (2015) 064102, https://doi.org/10.1063/1.4922859.
[19] S. Trasatti, O.A. Petrii, Real surface area measurements in electrochemistry, Pure Appl. Chem. 63 (1991) 711–734, https://doi.org/10.1351/pac199163050711.
[20] R. Notoya, A. Matsuda, Galvanostatic transient studies of platinum hydrogen electrode: application of periodic square current pulses, J. Res. Inst. Catalysis, Hokkaido Univ. 15 (1967) 247–255.

[21] K.R. Bickel, K.D. Etzel, V. Halka, R. Schuster, Microcalorimetric determination of heat changes caused by overpotential upon electrochemical Ag bulk deposition, Electrochim. Acta 112 (2013) 801–812, https://doi.org/10.1016/j.electacta.2013.06.056.
[22] L.E. Botello, M. Schönig, J. Solla-Gullón, V. Climent, J.M. Feliu, R. Schuster, Direct measurement of the hydrogen adsorption entropy on shape-controlled Pt nanoparticles using electrochemical microcalorimetry, J. Mater. Chem. A 12 (2023) 184–191, https://doi.org/10.1039/D3TA04937J.
[23] M. Schönig, S. Frittmann, R. Schuster, Identification of electrochemically adsorbed species via electrochemical microcalorimetry: sulfate adsorption on Au(111), Chemphyschem 23 (2022) 202200227, https://doi.org/10.1002/cphc.202200227.
[24] A. Lasia, Mechanism and kinetics of the hydrogen evolution reaction, Int. J. Hydrog. Energy 44 (2019) 19484–19518, https://doi.org/10.1016/j.ijhydene.2019.05.183.
[25] P.J. Rheinländer, J. Herranz, J. Durst, H.A. Gasteiger, Kinetics of the hydrogen oxidation/evolution reaction on polycrystalline platinum in alkaline electrolyte reaction order with respect to hydrogen pressure, J. Electrochem. Soc. 161 (2014) F1448–F1457, https://doi.org/10.1149/2.0501414jes.
[26] S. Frittmann, R. Schuster, Role of anions during the Cu underpotential deposition on Au(111): a microcalorimetric investigation, J. Phys. Chem. C 120 (2016) 21522–21535, https://doi.org/10.1021/acs.jpcc.6b06624.
[27] E.B. Tetteh, M. Kim, A. Savan, A. Ludwig, T.D. Chung, W. Schuhmann, Reassessing the intrinsic hydrogen evolution reaction activity of platinum using scanning electrochemical cell microscopy, Cell Rep. Phys. Sci. 4 (2023) 101680, https://doi.org/10.1016/j.xcrp.2023.101680.